Proceedings World Geothermal Congress 2026
Calgary, Canada, June 8 – 11, 2026

Hydraulic & Thermodynamic Modelling of Multilateral Closed-Loop Geothermal Systems

Erin Gillis*, Sara Eghbali[1] and Colin Brown[1]
Eavor Technologies Inc.[1]
Erin.gillis@eavor.com

Keywords: Geothermal, closed-loop geothermal, advanced geothermal systems, Eavor-Loop, thermodynamic modelling, hydraulic modelling, renewable energy, green energy

1 ABSTRACT

In the Eavor-Loop™ design, multilateral wellbores maximize heat transfer surface area between the circulating fluid and the surrounding rock. Mass flow rates in the laterals may vary and deviate from a uniform distribution, influenced by factors such as lateral geometry and rock and fluid thermophysical properties. This study presents a coupled fluid-flow and heat transfer simulation of water circulation in an Eavor-Loop™ with user-defined multilateral geometries. Pressure differences at lateral junctions are evaluated, and an objective function based on the pressure error at these nodes is defined. A gradient-based optimization algorithm is employed to determine the mass flow rate distribution across laterals. The impacts of trajectory design, operating time, flow rate, and inlet temperature on flow distribution and thermal production are analyzed.

Simulation results indicate that the flow distribution of an Eavor-Loop can deviate significantly from a uniform distribution in certain geometric and operational conditions. However, laterals with reduced flow rates yield higher fluid temperatures due to the increased residence time of the working fluid. The higher fluid temperatures offset the lower mass flow rates in a lateral. The overall impact of uneven flow distribution on the thermal output of an Eavor-Loop is minimal, illustrating the innate robustness of a closed-loop geothermal system. Thermal performance is most influenced by lateral length, followed by angle and manifold spacing. Uniform geometric changes across laterals have a greater effect than localized variations. Optimal performance is achieved with longer laterals, smaller (deeper) angles, and closer manifold spacing.

2 INTRODUCTION

The Eavor-Loop is a multilateral closed-loop geothermal system (CLGS) where a working fluid circulates through an underground heat exchanger to harvest thermal energy. Working fluid travels down an injection well until it reaches the target formation, at which point it splits into open-hole multilaterals to increase the heat transfer area. After the working fluid travels through the laterals and accumulates heat, the flow recombines at the bottom of the production well and flows to the surface. At surface, the geothermal heat can either be used for direct use or converted to electricity.

In the multilateral section, the flow rates are expected to be non-uniform. The flow rate through each lateral is governed by a balance of frictional and gravitational pressure changes. Gravitational pressure differences between the inlet and outlet arise from hydrostatic effects, which depend on fluid density and vertical height. As the fluid heats along each lateral, its density decreases, creating an upward gravitational pressure gain. When this gain exceeds frictional losses, the resulting buoyancy-driven circulation, known as the thermosiphon effect, drives flow without circulation pumping (Toews et al., 2020). Flow distribution is influenced by wellbore dimensions such as lateral length, depth and radius. To better understand fluid flow within the multilateral section, an algorithm was developed which numerically solves the flow distribution of an Eavor-Loop. This enables a clear understanding of how Eavor-Loop trajectory influences flow distribution, and consequently, Eavor-Loop production.

3 MODELLING METHODOLOGY

3.1 Transient model

The Eavor-Loop production over time can be predicted by solving the transient heat conduction between the surrounding rock and the wellbore fluid, along with the momentum and energy balance equations for the wellbore fluid. The Fourier heat conduction equation for the rock, considering transient heat conduction only and assuming negligible circumferential temperature variation, in a radial-cylindrical coordinate system (r, z) where z is the axial direction along the wellbore and r is the distance from the center of the well, is given by:

$$\rho c_{p,rock} \frac{\partial T}{\partial t} = \frac{1}{r}\frac{\partial}{\partial r}\left(r k_{rock} \frac{\partial T}{\partial r}\right) + \frac{\partial}{\partial z}\left(k_{rock} \frac{\partial T}{\partial z}\right) \quad (1)$$

Where ρ is fluid density in $\frac{kg}{m^3}$, $c_{p,rock}$ is rock heat capacity in $\frac{J}{kg \cdot K}$, and k_{rock} is rock thermal conductivity in $\frac{W}{m \cdot K}$.

The energy balance equation for the wellbore fluid in the one-dimensional (z) direction is given by:

$$\frac{\partial(\rho V h)}{\partial t} = \frac{\partial(\dot{m}(h+gy))}{\partial z} dz + q_{rf} \quad (2)$$

Where ρ is fluid density in $\frac{kg}{m^3}$, V is volume of control volume (m^3), h is fluid enthalpy ($\frac{J}{kg}$), $\dot{m}$ is fluid mass flow rate entering and exiting the control volume ($\frac{kg}{s}$), g is acceleration due to gravity (i.e., 9.81 $\frac{m}{s^2}$), y is the elevation or position of fluid in vertical direction parallel to gravity (m), and q_{rf} is the heat transfer rate from the rock face (W). This heat transfer is derived from the following equation:

$$q_{rf} = HA\left(T_{rw} - T_f\right) \quad (3)$$

Where H is convective heat transfer coefficient ($\frac{W}{m^2 \cdot K}$), A is the area of wellbore exposed to rock (m^2), T_{rw} is rock temperature at the wellbore ($°C$), T_f is wellbore fluid temperature ($°C$). At the interface between the rock and the fluid flowing through the loop, heat flux continuity is enforced; the heat flux calculated from Fourier's law in the rock must equal the heat flux entering the wellbore fluid:

$$q_{rf} = k_{rock} \frac{\partial T}{\partial r} = HA\left(T_{rw} - T_f\right) \quad (4)$$

Boundary conditions include inlet fluid temperature, pressure, and mass flow rate. The momentum balance equation for the wellbore fluid is given by:

$$\rho\left(\frac{\partial u}{\partial t} + u\frac{\partial u}{\partial z}\right) = -\frac{\partial P}{\partial z} + \mu\frac{\partial^2 u}{\partial z^2} + \rho g - f_{loss} \quad (5)$$

Where u is axial velocity ($\frac{m}{s}$), μ is dynamic viscosity ($Pa.s$), P is fluid pressure (Pa), f_{loss} is frictional loss per unit length ($\frac{N}{m}$). Assuming steady state momentum (i.e., $\frac{\partial u}{\partial t} = 0$), fully developed flow (i.e., $\frac{\partial^2 u}{\partial z^2} = 0$), uniform velocity across cross section (i.e., $\frac{\partial u}{\partial z} = 0$), and f_{loss} derived from Darcy-Weisbach equations (i.e., $f_{loss} = \frac{f_D \rho u^2}{2D}$ where f_D is Darcy friction factor, and D is wellbore diameter, m^2), fluid pressure can be calculated as follows:

$$\frac{\partial P}{\partial z} = \rho g - \frac{f_D \rho u^2}{2D} \quad (6)$$

The discretization of the equations and the solution scheme are explained in detail in Holmes et al., (2021) and Toews et al., (2020).

3.2 Flow split solution scheme

To accurately model the physics of the multilateral design, it is essential to consider that each lateral has its own unique geometry (e.g. inclination, depth, length). The mass flow rate in each lateral affects the fluid velocity, hydraulic pressure drop, and fluid pressure. Also, it directly affects heat transfer and fluid temperature as shown in Equation (2). Mass rate, pressure and temperature distributions will vary across laterals.

A schematic of the model is shown in Figure 1. Each fluid pathway consists of an injection manifold, production manifold and lateral open-hole section.

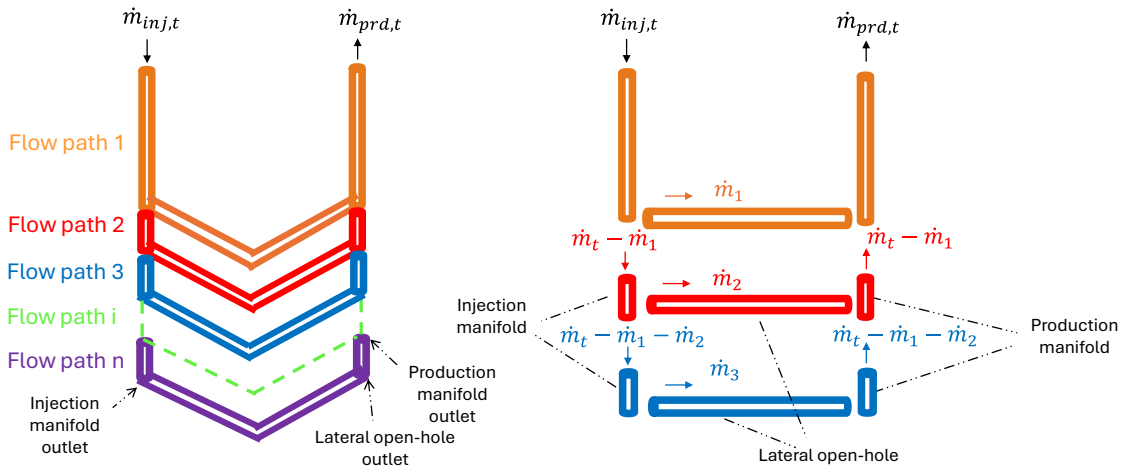


Figure 1: Schematic of multilateral loop in flow split simulation

As the inlet fluid travels down the injection well, the total mass flow rate, $\dot{m}_t$, is distributed among the various laterals based on hydraulics. Each lateral receives a portion of the total flow, denoted by $\dot{m}_i$ where:

$$\dot{m}_i = x_i \, \dot{m}_t \tag{7}$$

Here, x_i represents the loop flow fraction for lateral i, and $i = 1,2, \ldots, n$ with $i = 1$ being the shallowest (i.e., most upstream) and $i = n$ the deepest lateral (i.e., most downstream).

The temperature and pressure profiles along each lateral vary based on the flow rate $\dot{m}_i$, the lateral geometry, and the thermal properties of the surrounding rock. After passing through the lateral sections, the fluids from all laterals are gathered in the production manifold, and flow upward to the surface through the production well.

At each junction, where a lateral meets the production manifold, the pressure must be continuous. The pressure at the lateral outlet must equal the pressure in the production manifold section. To determine the correct mass flow rate distribution among laterals, an error function is defined based on pressure mismatches at the junctions. This error function must be minimized to obtain the loop flow fractions across all laterals.

$$Objective\ function = f\ (x_1, .., x_n) = \sqrt{\sum_{i=1}^{n-1} (P_{Prd-manif,out,i+1} - P_{Lat,out,i})^2} \tag{8}$$

Each flow pathway (denoted by the various colours in Figure 1 requires two mass flow rates: one for the manifold sections and one for the lateral open-hole section, as defined below:

$$\dot{m}_{i,Manif} = \dot{m}_t (1 - \sum_{j=1}^{i-1} x_j) \tag{9}$$

$$\dot{m}_{i,Lat} = x_i \, \dot{m}_t \tag{10}$$

Solving each segment requires specifying the inlet temperature and pressure as boundary conditions. For injection manifold segments, these inlet values are taken from the outlet conditions of the preceding (upstream) injection manifold. For the first fluid pathway, the inlet temperature and pressure correspond to the overall loop inlet conditions.

$$T_{Inj-manif,in,i} = T_{Inj-manif,out,i-1} \ \ for\ i = 2, .., n \tag{11}$$

$$T_{Lat,in,i} = T_{Inj-manif,out,i} \ \ for\ i = 1, .., n \tag{12}$$

$$P_{Inj-manif,in,i} = P_{Inj-manif,out,i-1} \ \ for\ i = 2, .., n \tag{13}$$

$$P_{Lat,in,i} = P_{Inj-manif,out,i} \ \ for\ i = 1, .., n \tag{14}$$

To find the inlet temperature of the production manifold segments for laterals 1 to n-1, a mass weighted average of the enthalpies at lateral outlet and production manifold outlet locations is used as follows:

$$h_{Prd-manif,in,\,i-1} = \frac{\dot{m}_{Lat,i-1} * h_{Lat,out,\,i-1} + \dot{m}_{Manif,i} * h_{Prd-manif,out,\,i}}{\dot{m}_{Lat,i-1} + \dot{m}_{Manif,i}} \ \ for\ i = n, .., 2 \tag{15}$$

$$P_{Prd-manif,in,\,i-1} = \frac{\dot{m}_{Lat,i-1} * P_{Lat,out,i-1} + \dot{m}_{Manif,i} * P_{Prd-manif,out,i}}{\dot{m}_{Lat,i-1} + \dot{m}_{Manif,i}} \; for\; i = n,..,2 \tag{16}$$

The objective function is non-linearly (implicitly) affected by the unknown mass rates within laterals. Therefore, a gradient descent optimization scheme is used (Nocedal and Wright, 2006).

The summation of all x_i must be equal to 1 and each must be a positive value between 0 and 1. For a loop with 12 laterals, the optimization problem involves 12 parameters constrained between 0 and 1, with their sum equal to 1. Directly using constrained optimization proved challenging due to the combination of bounds and equality constraints, which complicates gradient computations and can reduce solver stability. To simplify the problem, a softmax transformation was applied (Franke and Degen, 2022; Goodfellow et al., 2016), mapping unconstrained variables s_i from (−∞,+∞) to the [0,1] range while automatically enforcing the sum-to-one constraint as shown below. This approach allows all 12 parameters to be optimized independently (and unconstrained), improving numerical stability and convergence.

$$x_i = \frac{e^{s_i}}{\sum_{i=1}^{n} e^{s_i}} \; for\; i = 1,..,n \tag{17}$$

At each iteration, the s-variables are updated using Newton's method, based on the following equation:

$$s_{k+1} = s_k - H_k^{-1} * \nabla f(s_k) \tag{18}$$

Where s_k is softmax variables at k_{th} iteration, H_k and $\nabla f(s_k)$ are hessian and gradient of objective function evaluated at s_k.

3.3 Geological and Trajectory Definition

The following Table lists the geological and trajectory related inputs for the Eavor-Loop models presented within:

Table 1: Transient model inputs

Eavor-Loop Design Parameters		
Number of laterals	12	#
Eavor-Loop inlet temperature	50	°C
Eavor-Loop inlet pressure	2	MPa
Eavor-Loop flow rate	70	kg/s
Wellbore radius	0.108	m
Lateral section depth	4500	m
Lateral length	7000	m
Geological Parameters		
Geothermal gradient	30	°C/km
Rock thermal conductivity	3.2	W/m·K

4 ILLUSTRATIVE TRAJECTORIES

As mentioned above, during Eavor-Loop operation, the flow distribution amongst the laterals is not expected to be uniform. The multilateral section of an Eavor-Loop can be thought of as parallel flow paths in a hydraulic system. The parallel flow paths are highlighted in Figure 2 in varying colors:

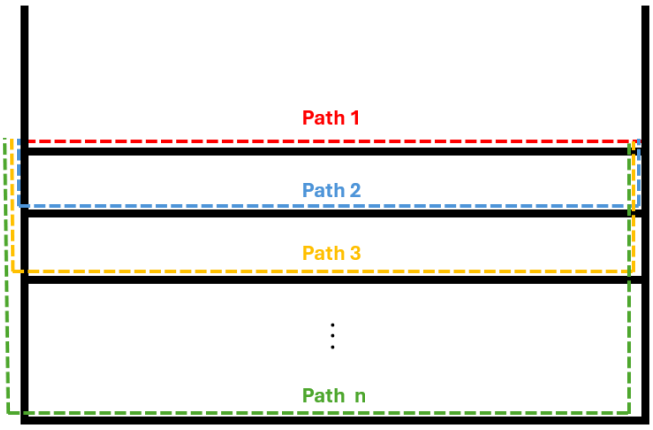


Figure 2: Equal pressure paths in multilateral section

With parallel flow paths, the flow will distribute itself such that the total pressure differential across each flow path is equal. The pressure differential along a flow path can be separated into two contributions, from frictional resistance and gravitational effects, as follows:

$$\Delta P_{tot} = \Delta P_{fric} + \Delta P_{grav} \tag{17}$$

Where ΔP_{fric} represents the pressure lost by the fluid as it flows due to viscous shear forces and ΔP_{grav} represents the hydrostatic pressure differential caused by gravity. In the direction of flow, ΔP_{fric} can only be a negative value, whereas ΔP_{grav} may be a positive or negative value depending on the change in density and/or elevation.

The balance between frictional and gravitational pressure differential across the parallel flow paths is what determines the flow distribution of an Eavor-Loop. In this section, incremental variations in Eavor-Loop trajectory will be presented to illustrate how these components of pressure drop influence the flow distribution of an Eavor-Loop. A typical Eavor-Loop multilateral trajectory is shown in the Figure below:

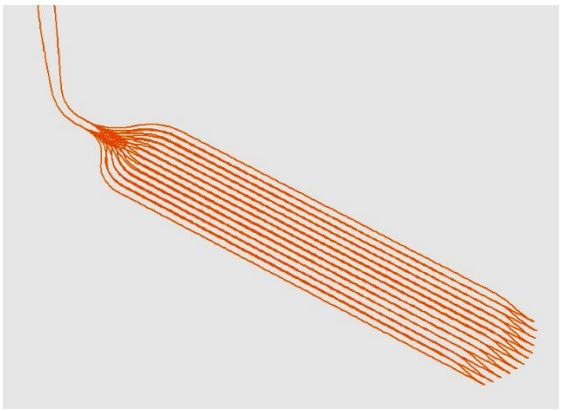


Figure 3: Realistic Eavor-Loop multilateral section trajectory

To isolate the effects of wellbore trajectory on lateral flow distribution, a simplified representative Eavor-Loop trajectory is used in this paper. The injection and production wells are at the same depths, and the laterals are completely straight. The representative trajectory is shown in Figure 4:

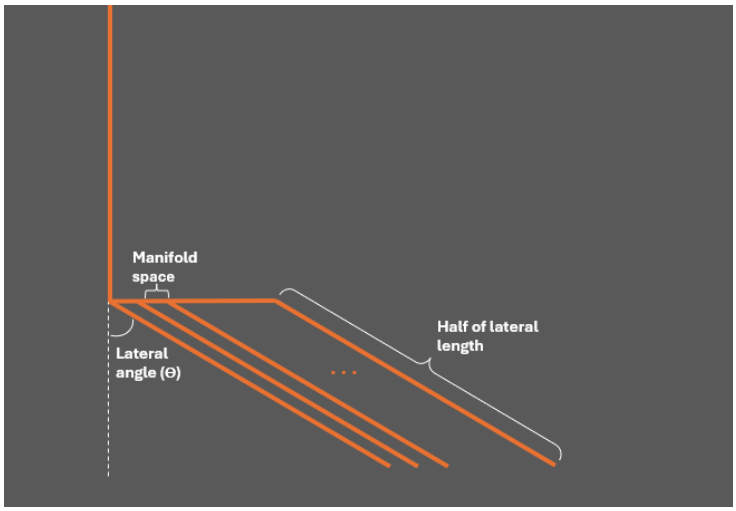


Figure 4: Simplified Eavor-Loop trajectory used in simulations

The following three cases will be explored: (1) 90° lateral angle and 0 m manifold space, (2) 90° lateral angle and 30 m manifold space, and (3) 85° lateral angle and 30 m manifold space. In each of these illustrative cases, the lateral length is the same for all laterals. The manifold section remains horizontal regardless of lateral angle, as demonstrated in Figure 4, such that the laterals experience the same rock temperature regardless of manifold spacing. The components of pressure differential in each lateral's flow path, as highlighted in Figure 2, are represented in the Figure below:

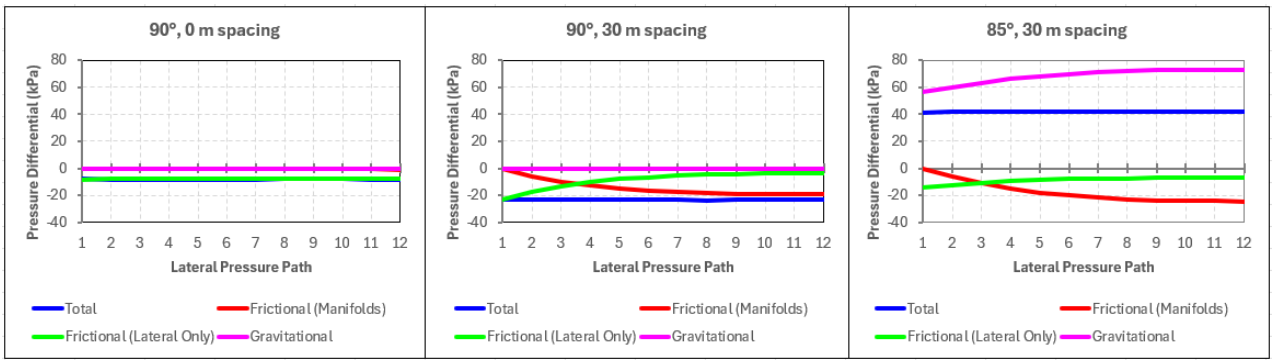


Figure 5: Lateral pathway pressure differential of illustrative trajectories

The resulting flow distributions are shown in the following Figure:

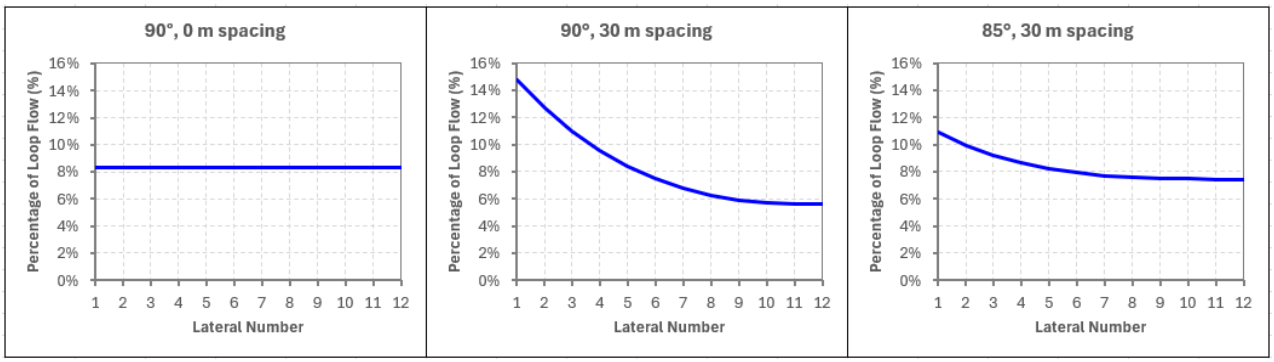


Figure 6: Flow distribution of illustrative trajectories

In the case of a 90° lateral angle, there is no gravitational pressure differential because there is no change in elevation in the lateral section. Further, if the manifold spacing is 0 m, there is no frictional pressure loss in the manifold section, therefore all the pressure difference comes from the frictional losses in the lateral section. Because the total pressure difference of each pathway must be equal, the flow rate in each lateral is equal.

When the lateral angle is maintained at 90° but the manifold spacing is increased to 30 m, the additional manifold length causes non-uniform hydraulic lengths. As illustrated in Figure 2, the pressure pathway for Lateral 1 has no manifold section, whereas the pressure pathway for Lateral 12 includes 660 m of manifold section. The frictional losses are split between the manifold and lateral portions. This results in a different flow rate in each lateral. As the flow travels from Lateral 1 to 12, the manifold frictional losses increase while the open-hole lateral frictional losses decrease. This is why in the 90° lateral angle and 30 m spacing case, Lateral 1 has approximately 15% of the loop flow, whereas Lateral 12 only has approximately 6% of the loop flow.

When the lateral angle is now reduced from 90° to 85°, the elevation difference within the lateral section enables a gravitational pressure gain, which acts in the opposite direction of frictional loss. The slower flow rate in Lateral 12 allows for more time for heat to be transferred to the working fluid, resulting in a higher gravitational pressure gain relative to the other laterals, as shown in Figure 3. This balance between gravitational and frictional pressure changes results in a more uniform flow distribution. In the 85° lateral angle and 30 m spacing case, Lateral 1 has approximately 11% of the loop flow, whereas Lateral 12 has approximately 7.5% of the loop flow.

Ultimately, the flow distribution of an Eavor-Loop is determined by a balance of frictional and gravitational pressure differentials. Manifold spacing induces a difference in frictional losses, causing a disproportionate amount of flow into Lateral 1 and the least amount of flow into Lateral 12. However, reducing the lateral angle below 90 degrees induces gravitational pressure changes within the laterals. The slower flow in Lateral 12 leads to an increased amount of gravitational pressure potential. This interaction between flow rate and heat transfer ultimately causes the Eavor-Loop to be resilient: differences in lateral length, manifold spacing and lateral angle can be accommodated because slower flow picks up more heat.

5 RESULTS

In this section, a sensitivity study is performed to investigate the impact of various geometric and operational parameters on loop flow distribution. The baseline Eavor-Loop being simulated is illustrated in Figure 4, and the geological and geometric parameters are listed in Table 1. An Eavor-Loop with an 85° lateral angle, 7000 m lateral length and 30 m manifold spacing is used as the base case.

5.1 Loop geometry impacts

5.1.1 Lateral length

Depending on the project, the lateral length may vary. This affects both the frictional and gravitational pressure changes, which may affect the distribution of flow. The flow distribution resulting from increasing or decreasing the lateral length by 800 m is shown in the Figure below:

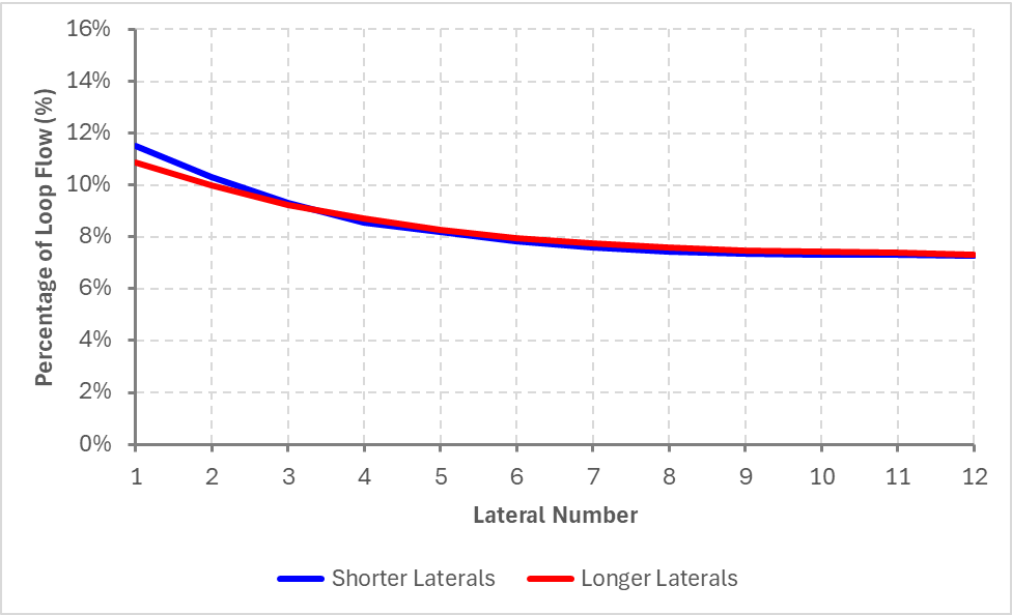


Figure 7: Effect of uniform lateral length on flow distribution

As seen in Figure 7, increasing the lateral length results in a more even flow distribution than decreasing the lateral length. This can be explained by the fact that longer laterals have more heat transfer area and experience higher rock temperatures, which increases the gravitational pressure contribution to the pressure differential.

There may be a discrepancy between the planned and as-drilled trajectories of the Eavor-Loop, resulting in non-uniform lateral length. The Figure below shows the flow distribution resulting from one lateral length being 800 m longer or shorter than the other laterals. The resulting flow distribution is shown below:

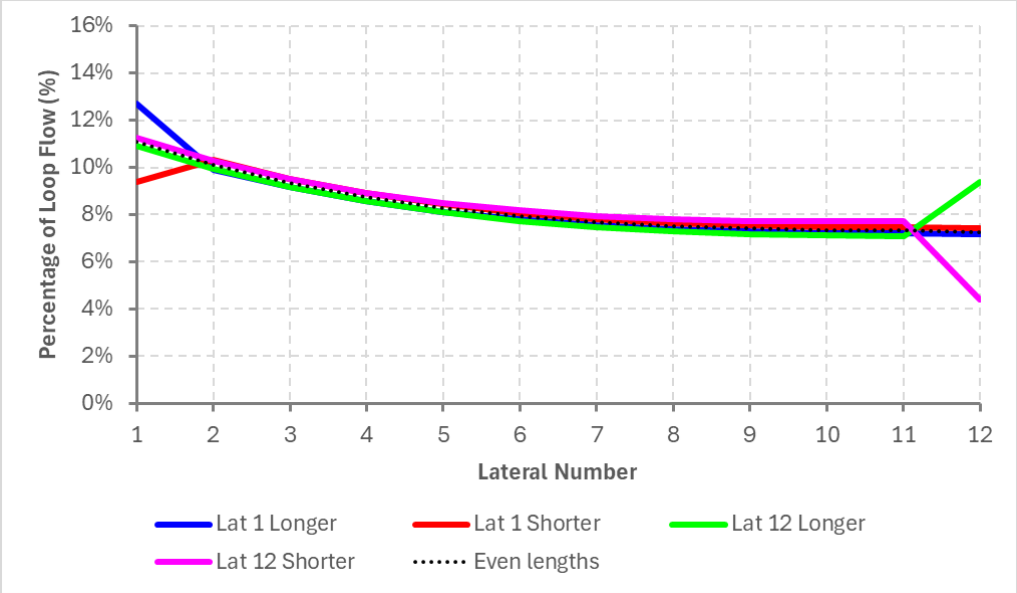


Figure 8: Flow distribution resulting from non-uniform lateral lengths

As shown in Figure 8, in the case of non-uniform lateral lengths, shorter laterals will have ~10-40% less flow rate relative to a uniform length trajectory, and the other laterals will take slightly more flow rate as a result. Conversely, longer laterals have more flow rate relative to a uniform length trajectory. A shorter lateral has less heat transfer area and experiences a colder maximum rock temperature because of a shallower maximum TVD. As a result, the reduced capacity for heat transfer in a shorter lateral leads to a smaller flow rate. Interestingly, in this example, length discrepancies occurring at lateral 12 have a higher impact to the flow distribution than length discrepancies at lateral 1. Shorter laterals result in 15% and 38% less flow in the lateral relative to a uniform trajectory for shorter laterals 1 and 12, respectively.

5.1.2 Manifold spacing

Manifold spacing is varied from 5 m to 60 m, and its impact on the flow distribution is analyzed, as shown in Figure 9. As manifold spacing increases, the fluid pathway to the downstream laterals becomes longer, leading to increased frictional pressure losses. Since this extended section of the manifold does not involve any change in true vertical depth (i.e., no associated rock temperature change), it contributes solely to additional flow

resistance. This increased resistance adversely affects flow distribution to the downstream laterals, resulting in a steeper flow split curve with increasing manifold spacing, as shown in Figure 9.

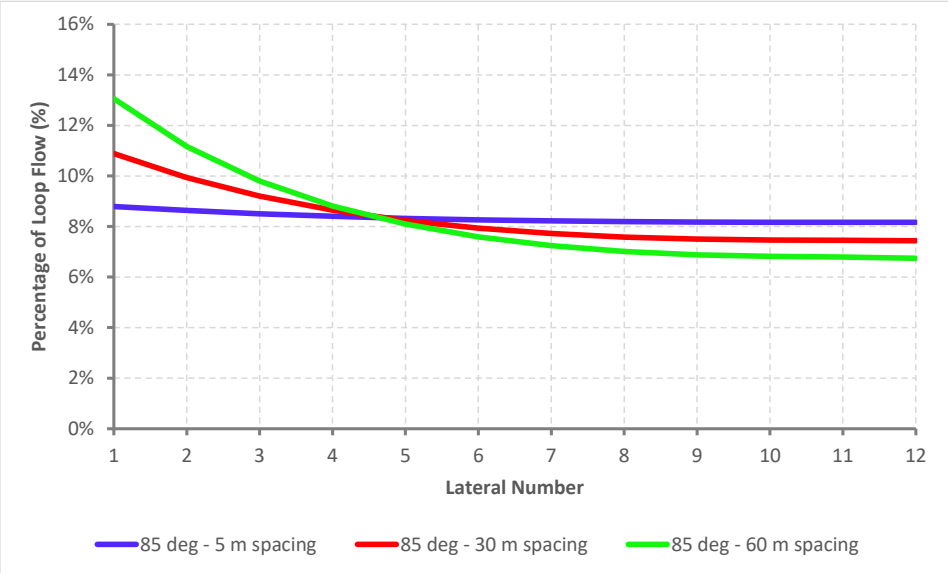


Figure 9: Effect of manifold spacing on flow distribution, after 1 year, 85 deg inclination

Increasing manifold spacing amplifies frictional losses in the injection and production manifold section of the downstream laterals, which leads to lower flow rates in these laterals. Overall, flow distribution is highly sensitive to manifold spacing. In the 60 m manifold spacing case, the flow rate in lateral 12 is almost 2 times as much as the flow rate in lateral 12, whereas the flow distribution is almost uniform for the 5 m manifold spacing case.

There may be a discrepancy between the planned and as-drilled trajectories of the Eavor-Loop, resulting in non-uniform manifold spacing. The Figure below shows the flow distribution resulting from one large 90 m manifold space. For exaggeration, it is assumed that this manifold spacing outlier occurs in the same location on both the injection and production manifolds. A lateral angle of 85° and a baseline manifold spacing of 30 m is used. The resulting flow distribution from non-uniform manifold spacing is shown below:

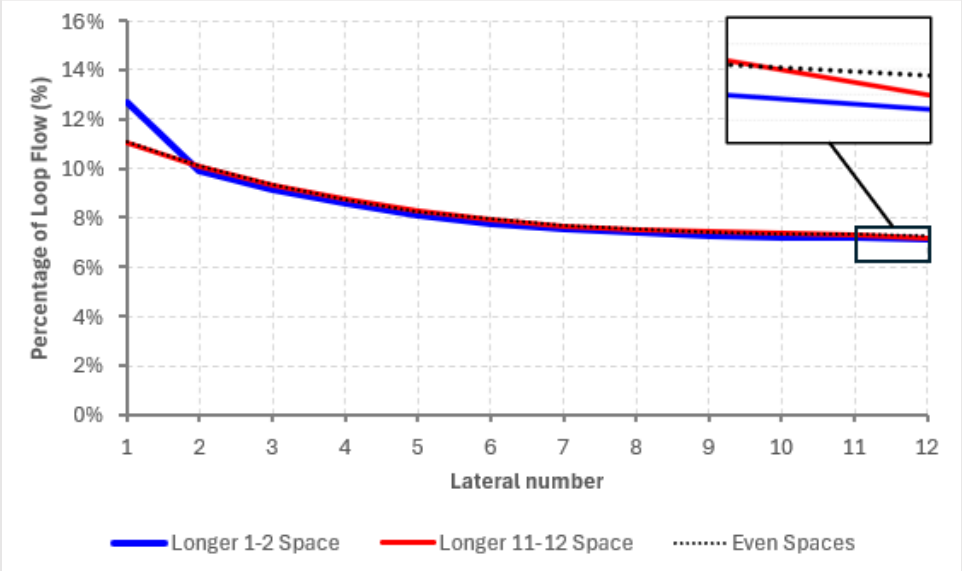


Figure 10: Flow distribution from non-uniform manifold spacing

As shown in Figure 10, a large manifold spacing at lateral 1 results in a more discontinuous flow split, with a high flow rate entering lateral 1. The same manifold spacing after lateral 11 results in a more uniform flow distribution. This can be explained by the difference in frictional losses between the manifold segments, driven by the difference in fluid velocity. The fluid velocity in the lateral 1-2 manifold space is roughly 12 times higher than the

velocity in the lateral 11-12 manifold space. Due to the location, if the manifold space after lateral 1 is longer, the manifold frictional losses for laterals 2-12 increase, thereby reducing their flow rate. If the manifold space after lateral 11 is longer, the remaining laterals' manifold frictional losses are unaffected, and lateral 12 flow rate is only slightly reduced.

5.1.3 Lateral angle

Lateral inclination was varied from 20° to 85° to investigate its effect on flow distribution. A lateral angle of 91° is also presented to illustrate the impacts of a "toe-up" configuration. illustrates the flow distribution after one year, across various inclinations:

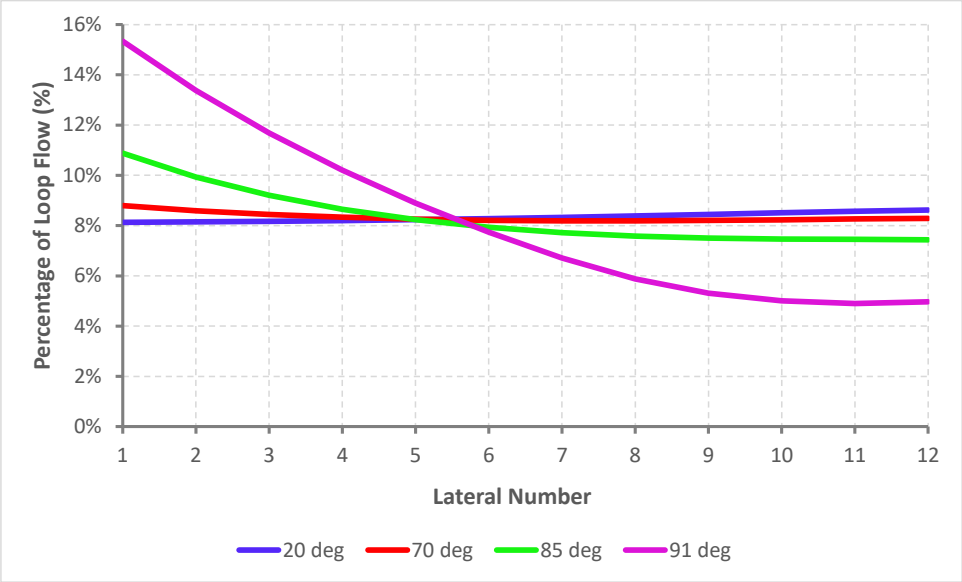


Figure 11: Effect of inclination on flow distribution after 1 year

The exposure to hotter rock leads to a substantial increase in gravitational pressure gain across all laterals (i.e. intra-lateral thermosiphon). With varying inclination, the frictional losses remain relatively unchanged as total flow path length is the same. However, the ratio of gravitational driving force to frictional resistance increases significantly as the inclination decreases. This change favors downstream laterals, allowing them to carry a greater flow rate despite their longer flow paths and higher frictional losses. As a result, upstream lateral flow rates decrease while downstream lateral flow rates increase, leading to a more balanced distribution among all laterals.

At 20° inclination, flow distribution becomes nearly uniform. This evening-out is driven by an enhanced thermosiphon effect, as fluids are exposed to deeper, hotter rock, generating stronger buoyancy forces. After one year, the pressure gain in Lateral 2 is 1.35 MPa at 20° inclination compared to only 0.05 MPa at 85°, while the corresponding temperature gains are 102.5°C and 64.3°C, respectively.

There may be a discrepancy between the planned and as-drilled trajectories of the Eavor-Loop, resulting in non-uniform lateral angles. This section will explore the flow distribution resulting from one lateral angle being +/- 1° different from the rest. The flow distributions from laterals 1 or 12 being drilled at a different lateral angle is shown below:

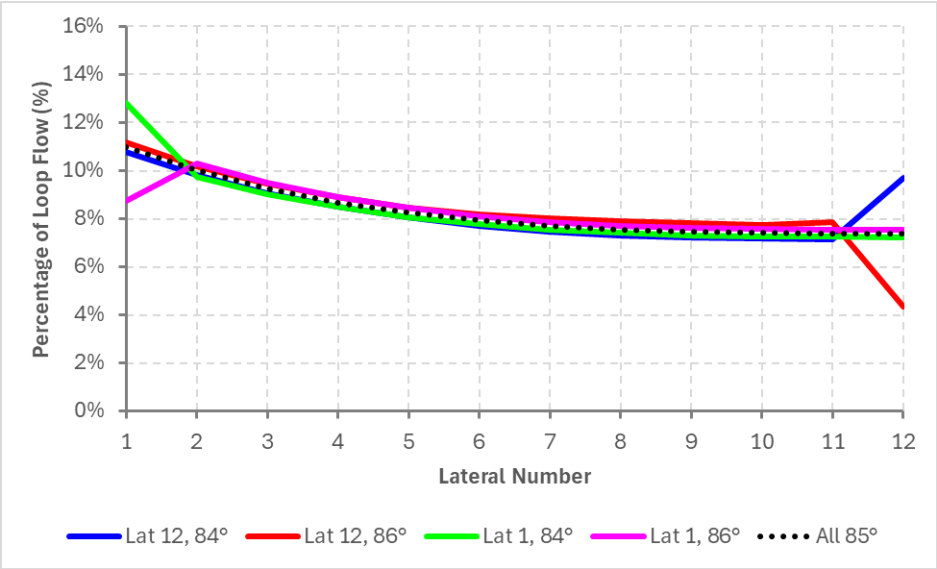


Figure 12: Flow distribution from non-uniform lateral angles

As shown in Figure 12, decreasing lateral angles (more towards the vertical) result in increased flow rate to the deviated lateral, and increasing lateral angles (more towards horizontal) results in decreased flow rate to the deviated lateral. Increasingly vertical lateral trajectories interact with higher rock temperatures due to the increased TVD. Therefore, deeper laterals experience more heat transfer and can accommodate increased flow as a result due to the intra-lateral thermosiphon. The opposite effect is true if a lateral is drilled at a higher angle than the others. Our analysis suggests that Lateral 12 is slightly more sensitive to angle discrepancies than Lateral 1.

5.2 Operational Impacts

5.2.1 Time

The effect of operating time on flow distribution and production performance is shown in the below Figure:

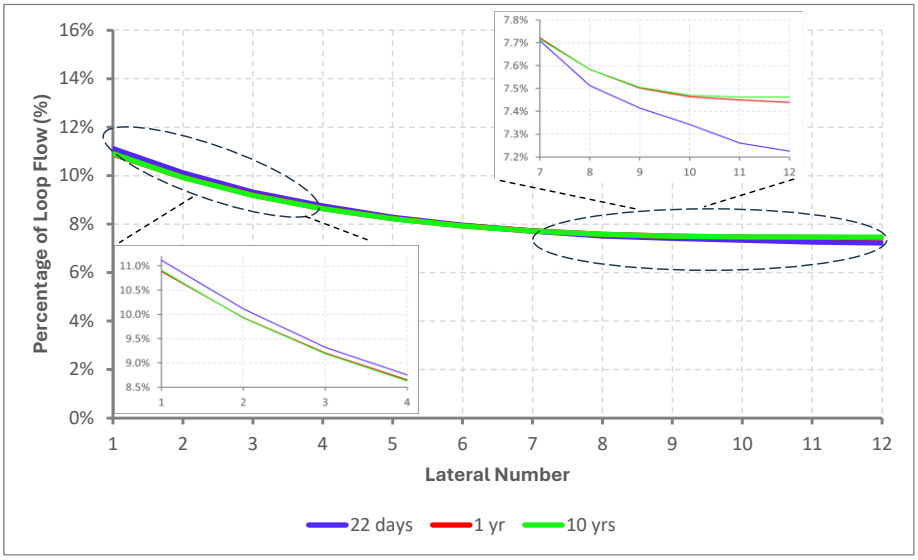


Figure 13: Effect of time on flow distribution

Initially, the fluid temperature in the laterals closely follows that of the surrounding rock (i.e. not much of a temperature gradient across the laterals). As injection continues, the temperature gain along the laterals increases, driving a stronger thermosiphon effect and increasing the gravitational driving force. Early on, downstream laterals with longer flow paths carry lower flow rates due to higher frictional losses (with no significant intra-lateral thermosiphon to offset it). Over time, as buoyancy forces grow and overcome friction, these laterals carry higher flow rates, leading to a more uniform flow distribution. Once the fluid temperature

gradient along the lateral reaches steady state, the flow distribution remains nearly unchanged with time. Overall, operating time has an insignificant effect on flow distribution.

5.2.2 Flow rate

The operating flow rate of an Eavor-Loop may vary between projects, or throughout a project's life per the operating strategy. The flow distribution of an Eavor-Loop at a lateral angle of 85° at different flow rates is shown below:

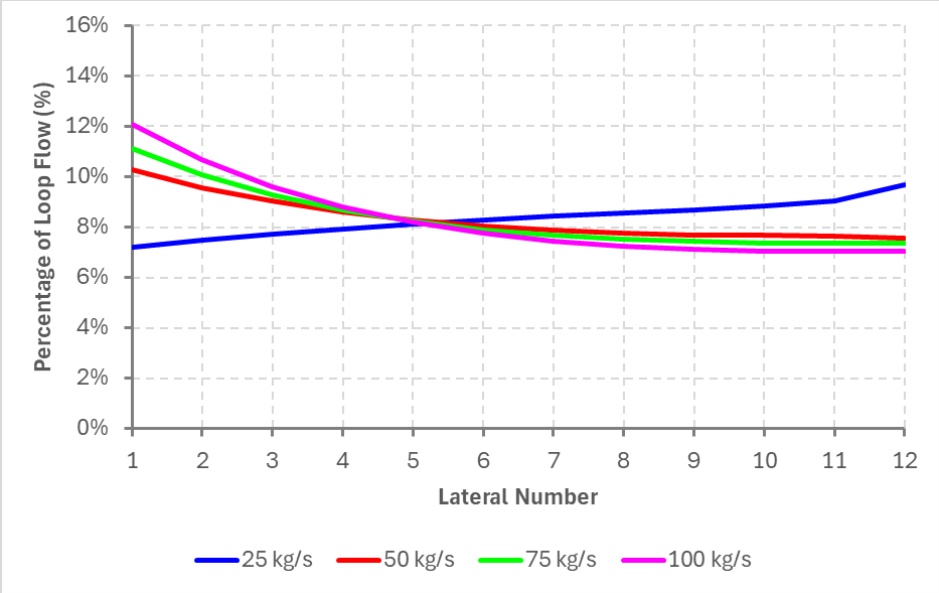


Figure 14: Flow distribution resulting from various loop flow rates

As shown in Figure 14, the lateral with the highest flow percentage is lateral 12 at low flow rates, and lateral 1 at high flow rates. At low flow rates, hydraulic losses are small as hydraulic losses are proportional to the square of fluid velocity. Therefore, gravitational pressure differential dominates the flow distribution, requiring more flow into lateral 12. When the loop flow rate is sufficiently high, the hydraulic pressure loss competes with the gravitational pressure gain, thereby reversing the flow distribution to require the most flow into lateral 1.

As the flow rate increases beyond 50 kg/s, the hydraulic losses increase while the residence time of the working fluid in the multilateral section decreases, thereby reducing the gravitational pressure gain. Therefore, higher loop flow rates result in a flow distribution which increasingly favors lateral 1. As the loop flow rate increases from 50 kg/s to 100 kg/s, the flow distribution becomes increasingly unbalanced, with more flow rate entering laterals 1-4 and less entering laterals 5-12.

5.2.3 Inlet temperature

The flow distribution of an Eavor-Loop at a lateral angle of 85° operating with different inlet temperatures is shown below:

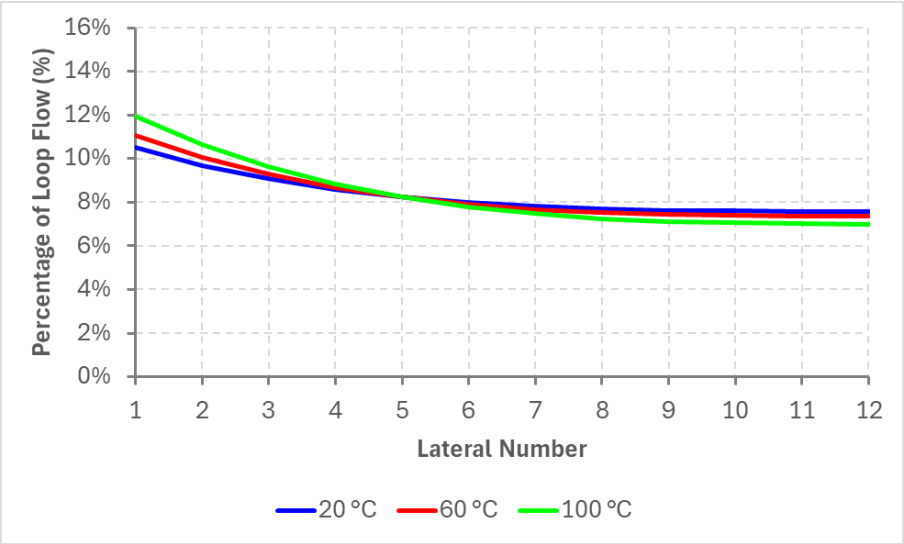


Figure 15: Flow distribution resulting from various injection temperatures

Lower injection temperatures result in a more uniform flow distribution. This is because a lower injection temperature results in an increased amount of heat transfer in the laterals (higher temperature gradient along the laterals), which increases the gravitational pressure differential in each lateral, thereby producing a more uniform flow distribution. Overall, the flow distribution is relatively insensitive to injection temperature.

5.3 Thermal Production Impact

5.3.1 Geometric feature summary

This paper has illustrated how different Eavor-Loop geometric features such as lateral length, manifold spacing and lateral angle influence the flow distribution. These features also have an impact on the thermal output of the Eavor-Loop. A tornado chart illustrating the overall impacts of loop geometry features on production is shown below:

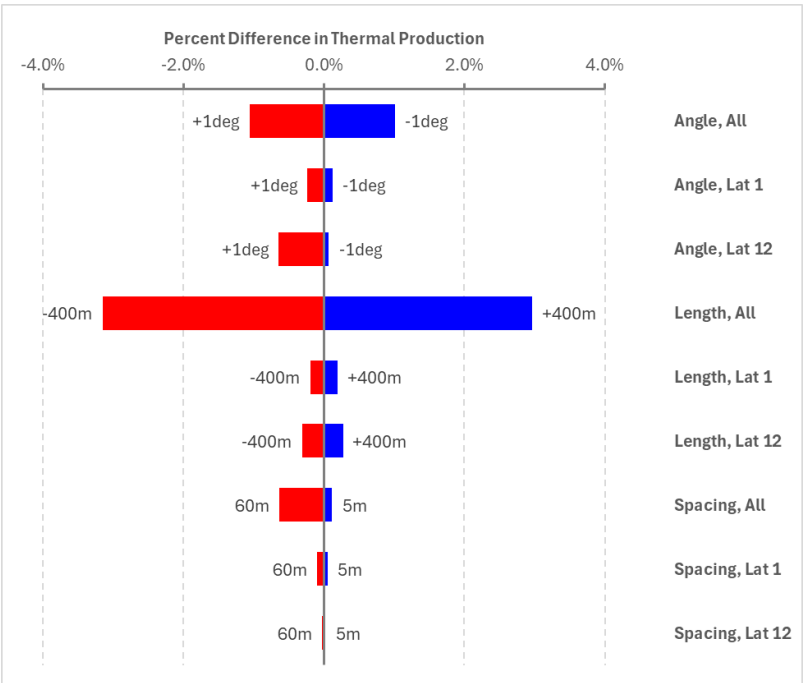


Figure 16: Impact of loop geometry changes on thermal production (19.8 MW baseline case: 85° angle, 7000 m length and 30 m manifold spacing)

Figure 16 demonstrates the impact of geometry changes on loop thermal output. The geometric feature with the greatest impact on thermal production is lateral length, followed by lateral angles and manifold spacing. For

lateral angle, length and manifold spacing, varying all the laterals together has more of an impact to production than varying a single lateral.

When only one lateral varies, the lateral number may be impactful. For the lateral angle, it is imperative to avoid an increased lateral 12 angle, which causes a 0.6% production loss, but only a 0.2% production loss is caused by an increased lateral 1 angle. For lateral length, production impact is also more sensitive to changes in lateral 12 length than lateral 1. Conversely, for manifold spacing, production impact is more sensitive to changes in the lateral 1-2 spacing than the 11-12 spacing. Manifold spacing is relatively insensitive to a single increased manifold spacing (~0.1% change in production), but if all the manifold spacings increase from 30 m to 60 m there is a 1% decrease in loop production.

As shown in Figure 16, trajectory changes significantly impact loop thermal production. The thermal production of an Eavor-Loop can be optimized by implementing the following:

- Minimize the lateral angle. Monitor directional drilling closely to avoid trajectories which approach or exceed an inclination of 90°. Lower lateral angles lead to higher thermal production.
- Maximize the lateral length. Longer laterals lead to higher thermal production.
- Minimize the manifold spacing. Large manifold spacings lead to reduced thermal production.

Across all scenarios, the cases exhibiting greater non-uniformity in flow distribution also exhibit lower thermal production. However, in these cases it is difficult to isolate the impact of flow distribution alone on thermal production, because the geometric features inherently impact production. For example, a loop with a lateral angle of 84° has a more uniform flow distribution as well as higher thermal production relative to a lateral angle of 85° degrees. A lateral angle of 84° would have higher rock temperatures due to a deeper TVD, leading to an increase in thermal production. The impact of flow distribution on production cannot be isolated in this case.

5.3.2 Flow distribution impact in isolation

The impact of non-uniform flow distribution on thermal production can be isolated by comparing the thermal output corresponding to the solved flow distribution with that of an equivalent uniform flow distribution for the same Eavor-Loop configuration. To investigate this, the baseline trajectory of 85° lateral angle, 7000 m lateral length and 30 m manifold was simulated, once with the solved flow distribution and once with a uniform flow distribution. The lateral outlet temperatures and mass flow rates are shown in the figure below:

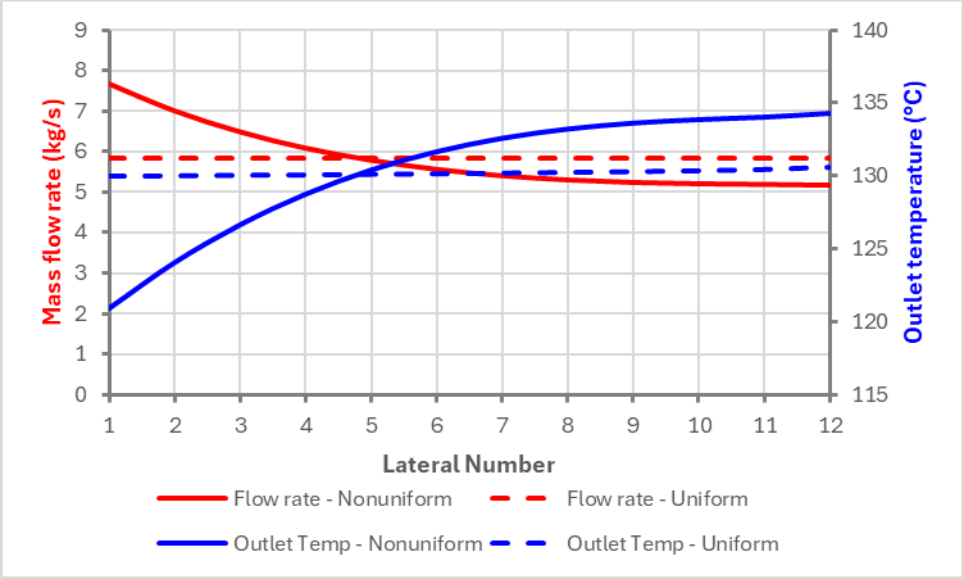


Figure 17: Lateral flow rate and outlet temperature for a uniform and nonuniform flow distribution

As seen in Figure 17, in the nonuniform flow distribution case, there is an inverse relationship between lateral flow rate and outlet temperature. Laterals operating at lower flow rates have longer fluid residence times, allowing more heat transfer from the surrounding rock to the working fluid and resulting in higher outlet temperatures. For example, although the flow rate in Lateral 1 is approximately 1.5 times greater than that in Lateral 12, the outlet temperature of Lateral 12 is 15 °C higher than Lateral 1. The total thermal production from each loop is shown in the following figure:

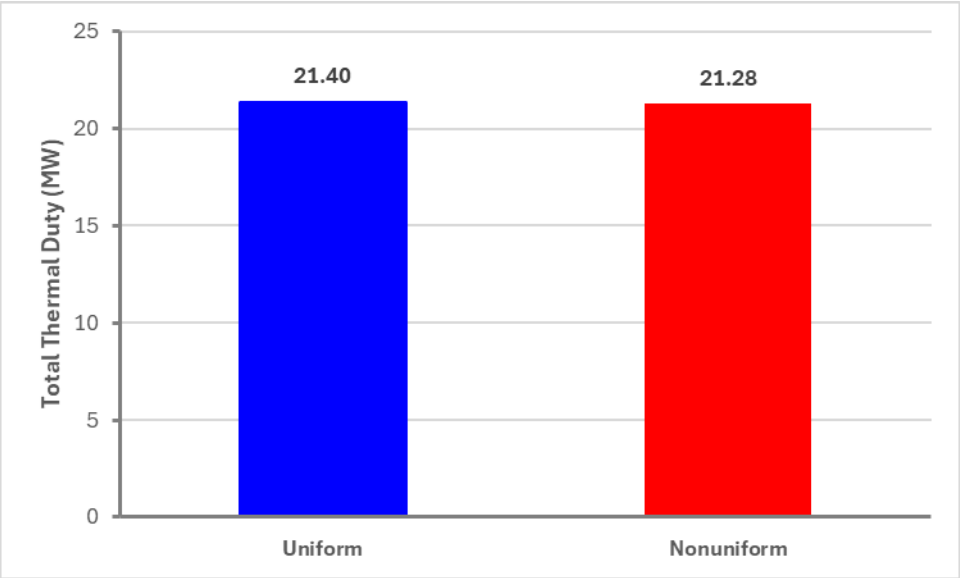


Figure 18: Total loop thermal production under uniform and non-uniform flow distributions

As shown in Figure 18, flow distribution within the Eavor-Loop has a minimal impact on overall thermal production. The non-uniform flow case produces only 0.5% less thermal energy than the uniform flow case.

6 CONCLUSION

A transient fluid-flow and heat transfer study was conducted on a multilateral Eavor-Loop design to quantify flow distribution among laterals and assess the effects of geometric and operating parameters.

Flow distribution among the laterals is governed by the interplay between frictional and gravitational pressure changes, both of which are strongly influenced by wellbore geometry, including lateral length, depth, angle, and manifold spacing. In general, frictional pressure losses within the manifold promote flow maldistribution, while intra-lateral thermosiphon effects partially offset this tendency.

Although geometric variations can produce substantial differences in lateral flow rates, the resulting impact on thermal production is small. Lower-flow laterals achieve higher outlet temperatures due to increased residence times, compensating for their reduced flow rates. Consequently, even in cases with significant flow maldistribution, total loop thermal production remains largely unchanged. Thermal production is more sensitive to the design parameter itself than to the resulting changes in flow distribution.

Overall, the impact of Eavor-Loop flow maldistribution on total thermal production is minimal, demonstrating the inherent robustness of the closed-loop system. Understanding how geometry and operating conditions shape flow distribution provides valuable guidance for optimizing Eavor-Loop design and performance.

7 REFERENCES

Franke, Markus, & Degen, Johannes. (2023). *The Softmax Function: Properties, Motivation, and Interpretation*. Preprint, Stanford ALPS Lab. https://alpslab.stanford.edu/papers/FrankeDegen_submitted.pdf

Goodfellow, Ian, Bengio, Yoshua, & Courville, Aaron. (2016). *Deep Learning*. MIT Press.

Holmes, Michael, Toews, Matthew, Jenkins, Jesse, & Sepulveda, Nestor. (2021). Multilateral closed-loop geothermal systems as a zero-emission load-following resource. *GRC Transactions*, 45, 25–52.

Nocedal, Jorge, & Wright, Stephen J. (2006). *Numerical Optimization* (2nd ed.). Springer.

Toews, Matthew, Riddell, Derek, Vany, Jeanine, & Schwarz, Bailey. (2020). Case study of a multilateral closed-loop geothermal system. In *Proceedings, World Geothermal Congress*, Reykjavik, Iceland, April.